LANGMUIR

Article

pubs.acs.org/Langmuir

A Blue-Light-Emitting BODIPY Probe for Lipid Membranes

Mihaela Bacalum,[†,‡] Lina Wang,[§,◆] Stijn Boodts,[§] Peijia Yuan,[§,¶] Volker Leen,[§] Nick Smisdom,[†] Eduard Fron,[§] Stefan Knippenberg,[†,∥] Gabin Fabre,[⊥,#] Patrick Trouillas,[#,∇,○] David Beljonne,[○] Wim Dehaen,[§] Noël Boens,[§] and Marcel Ameloot*[,†]

[†]Biomedical Research Institute, Hasselt University, Agoralaan Building C, 3590, Diepenbeek, Belgium

[‡]Department of Life and Environmental Physics, Horia Hulubei National Institute for Physics and Nuclear Engineering, Reactorului 30, Măgurele, 077125, Romania

[§]Department of Chemistry, Katholieke Universiteit Leuven (KU Leuven), Celestijnenlaan 200f - bus 02404, 3001 Leuven, Belgium

[∥]Division of Theoretical Chemistry and Biology, KTH Royal Institute of Technology, School of Biotechnology, Roslagstullsbacken 15, S-106 91 Stockholm, Sweden

[⊥]LCSN-EA1069, Faculté de Pharmacie, Université de Limoges, 2, rue du Dr. Marcland, 87025 Limoges Cedex, France

[#]Regional Centre of Advanced Technologies and Materials, Department of Physical Chemistry, Faculty of Science, Palacký University, tř. 17 listopadu 12, 771 46 Olomouc, Czech Republic

[∇]INSERM UMR-S850, Faculté de Pharmacie, Université de Limoges, 2 rue du Docteur Marcland, 87025 Limoges Cedex, France

[○]Service de Chimie des Matériaux Nouveaux, Université de Mons, Place du Parc 20, B-7000 Mons, Belgium

Supporting Information

ABSTRACT: Here we describe a new BODIPY-based membrane probe (**1**) that provides an alternative to dialkylcarbocyanine dyes, such as DiI-C_{18}, that can be excited in the blue spectral region. Compound **1** has unbranched octadecyl chains at the 3,5-positions and a *meso*-amino function. In organic solvents, the absorption and emission maxima of **1** are determined mainly by solvent acidity and dipolarity. The fluorescence quantum yield is high and reaches 0.93 in 2-propanol. The fluorescence decays are well fitted with a single-exponential in pure solvents and in small and giant unilamellar vesicles (GUV) with a lifetime of ca. 4 ns. Probe **1** partitions in the same lipid phase as DiI-C_{18}(5) for lipid mixtures containing sphingomyelin and for binary mixtures of dipalmitoylphosphatidylcholine (DPPC) and dioleoylphosphatidylcholine (DOPC). The lipid phase has no effect on the fluorescence lifetime but influences the fluorescence anisotropy. The translational diffusion coefficients of **1** in GUVs and OLN-93 cells are of the same order as those reported for DiI-C_{18}. The directions of the absorption and emission transition dipole moments of **1** are calculated to be parallel. This is reflected in the high steady-state fluorescence anisotropy of **1** in high ordered lipid phases. Molecular dynamic simulations of **1** in a model of the DOPC bilayer indicate that the average angle of the transition moments with respect to membrane normal is ca. 70°, which is comparable with the value reported for DiI-C_{18}.

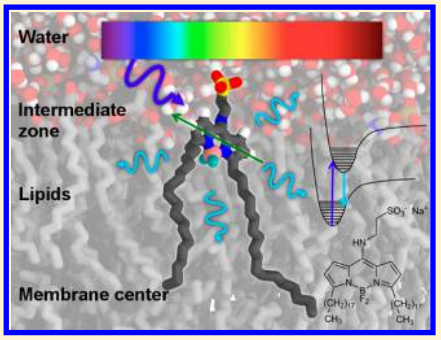

INTRODUCTION

There is an ever-growing interest in using compounds derived from 4,4-difluoro-4-bora-3*a*,4*a*-diaza-*s*-indacene (BODIPY) in life-science research.[1−4] The popularity of BODIPY dyes is due to a combination of outstanding spectroscopic and (photo)-physical properties, such as bright fluorescence with absorption and emission bands in the visible range, high molar absorption coefficients, and robustness toward light and chemicals. Moreover, the BODIPY core can be postfunctionalized easily[5] (at the pyrrole ring positions, the *meso*-position, and the boron atom), leading to dyes with custom-made, fine-tuned spectroscopic properties for use in biosciences and material research.

Lipid systems (e.g., bilayers, monolayers, vesicles, biological membranes) can be studied by inserting fluorescent probes.[6] BODIPY is one of the fluorophores frequently used to synthesize lipid probes.[7−14] These probes are anchored within the lipid membrane by 1, 2, or 3 hydrocarbon chains. The BODIPY core can be attached at different positions along the hydrocarbon chain. Additional alkyl chains attached to the fluorophore moiety lead to a deeper and more defined location of the probe in the lipid bilayer but the orientation of the electronic transition dipole moment of the fluorophores depends on the phase of the lipid membrane.[8]

Phospholipid bilayers exist in various phases according to lipid composition and temperature.[15] Pure phospholipid systems at temperatures below their phase transition temperature (T_m) exist in the gel phase (S_o), which is characterized by

Received: February 6, 2016
Revised: March 21, 2016
Published: March 22, 2016

DOI: 10.1021/acs.langmuir.6b00478
Langmuir 2016, 32, 3495−3505

dense packing and low lipid mobility.[15] Above T_m, the lipids are found in a liquid-crystalline phase (L_d) characterized by loose packing and high lipid mobility.[15] Mixing two phospholipids with different T_m leads to S_o/L_d phase coexistence.[16] When sphingomyelin (SM) and cholesterol (Chol) are added to glycerol-based phospholipids with low T_m, a phase separation can be observed[16] between the L_d phase consisting mostly of phospholipids and the liquid ordered phase (L_o) phase enriched in SM and Chol. L_o/L_d phase separation can be also obtained by mixing DOPC (a lipid with low T_m), DPPC (a lipid with high T_m) and Chol. The L_o phase can be considered as an intermediate phase between S_o and L_d because it preserves properties from both of them, that is, a high order of acyl-chains similar to the S_o phase, and a high lateral mobility similar to the L_d phase.

The aim of this work is to develop a new, highly fluorescent BODIPY-based lipid probe that (i) allows for the observation of lipid membranes at orientations perpendicular to the excitation beam; (ii) exhibits sensitivity to the different lipid phases; and (iii) can be excited in the blue spectral region. A well-defined orientation of the fluorescent probe that can be used in the blue spectral region in combination with a synthesis that allows for different lengths of hydrocarbon chains opens new alleys and combinations of dyes and proteins to explore membrane properties, lipid−lipid, and lipid−protein interaction. The observation of lipid membranes perpendicular to the excitation beam requires transition dipole moments ($S_1 \leftarrow S_0$ transition) of lipid probes to be nearly parallel to the membrane surface. Otherwise, the excitation probability will be substantially reduced because of the low photoselection probability due to the large angle between the electric field of the excitation light and absorption transition dipole moment.[17]

Theoretical studies[18] indicate that the first transition state dipole moment of BODIPY lies in the plane of the molecule and points from one terminal ring to the other. To obtain the proper orientation of the dipole moment of the aimed molecule with respect to the membrane, we were inspired by the long-chain dialkylcarbocyanine dyes DiI-C_{18}(3) (1,1′-dioctadecyl-3,3,3′,3′-tetramethylindocarbocyanine perchlorate) and DiI-C_{18}(5) (1,1′-dioctadecyl-3,3,3′,3′-tetramethylindodicarbocyanine perchlorate) which fluoresce, respectively, in the orange and red part of the spectrum and have similar membrane properties.[19] It has been shown that the great majority of the conjugated bridge of DiI-C_{18}(3) is within approximately 10% of parallelism with the surface of the cell membrane.[20] These probes also show lipid phase sensitivity toward S_o and L_d phases, depending on the lipid composition of the vesicles.[21−23]

Blue-shifted dyes are amenable to both single- and two-photon excitation, which makes these dyes very promising in a broad range of biological applications. Classic BODIPY derivatives generally fluoresce in the green spectral range[2−5] but careful choice of substituents can result in fluorescence emission in the yellow, red, and even near-IR parts of the spectrum.[2−5] Biellmann et al. reported the first *meso*-amino substituted BODIPY derivative, 8-phenylaminoBODIPY with absorption in the blue spectral range,[24] but with practically no fluorescence emission. Later, several *meso*-aminoBODIPY derivatives have been described with bright blue fluorescence.[25−29] Therefore, a membrane probe based on a *meso*-amino substituted BODIPY is expected to exhibit spectra lying in the blue spectral region.

Here we describe the new probe **1** (sodium 8-[(2-sulfonatoethyl)amino]-4,4-difluoro-3,5-dioctadecyl-4-bora-3*a*,4*a*-diaza-*s*-indacene, Figure 1) with two C_{18}-alkyl chains at the 3,5- positions and a taurine substituent at the *meso*-position.

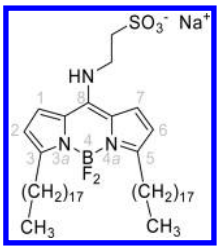

Figure 1. Structure of the BODIPY-based membrane probe **1**. The numbering of the BODIPY core is shown in gray.

The spectroscopic and photophysical properties of **1** in solvents of widely varying properties are investigated first, using UV−vis spectrophotometry and steady-state and time-resolved fluorometry. Second, the probe's behavior was investigated in model lipid systems, namely small (SUV) and giant (GUV) unilamellar lipid vesicles of different compositions. The probe's partitioning into binary and ternary lipid mixtures exhibiting phase separation was analyzed by fluorescence microscopy. Third, molecular dynamics simulations were used to describe both the location and orientation of **1** at the molecular level in a model lipid bilayer, as well as the geometrical characterization of its transition dipole moment. Finally, we performed fluorescence lifetime imaging microscopy (FLIM) of **1** in the membrane of OLN-93 cells. The lateral diffusion of **1** was determined in both GUV membranes and the plasma membrane of OLN-93 cells.

EXPERIMENTAL SECTION

The Supporting Information describes in detail the chemicals used in the experiments, the instrumentation used for spectrophotometry and steady-state and fluorescence spectroscopy, the relative determination of the fluorescence quantum yields, the small and giant unilamellar vesicles preparation, the cell culture, the techniques of fluorescence spectroscopy, single-photon timing (SPT), fluorescence up-conversion, fluorescence lifetime imaging microscopy (FLIM), fluorescence recovery after photobleaching (FRAP) and raster image correlation spectroscopy (RICS), and the molecular dynamics (MD) simulations. Here are the abbreviations of the chemical compounds used: dipalmitoylphosphatidylcholine = DPPC, dioleoylphosphatidylcholine = DOPC, distearoylphosphatidylcholine = DSPC, dimethylformamide = DMF, dimethyl sulfoxide = DMSO, tetrahydrofuran = THF, and methanol = MeOH. Additional details are provided as Supporting Information.

RESULTS

Synthesis of 1. The BODIPY-based membrane probe **1** (Figure 1) was prepared based on the method of Biellmann et al.[24] Full details are given in the Supporting Information. Briefly, 2-octadecylpyrrole **2** was condensed with thiophosgene in diethyl ether to yield the corresponding thioketone. This intermediate was not purified due to its unstable nature. The S-methylation to a dipyrrinium salt and the subsequent complexation with boron trifluoride etherate were carried out in a one-pot procedure. The brightly fluorescent dye **3** was then converted into the membrane probe **1** by nucleophilic substitution of the thiomethyl substitutent by taurine (Scheme 1). It should be noted that following a new synthetic route **1** can also be prepared by nucleophilic substitution of 8-

DOI: 10.1021/acs.langmuir.6b00478
Langmuir 2016, 32, 3495−3505

Scheme 1. Synthesis of 1[a]

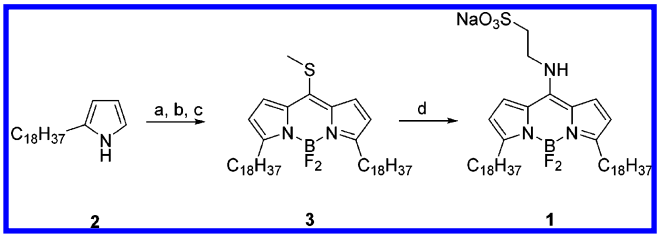

[a](a) $CSCl_2$, diethyl ether/toluene; (b) CH_3I, CH_2Cl_2; (c) NEt_3, $BF_3{\cdot}OEt_2$, CH_2Cl_2; (d) Taurine, DMSO/CH_2Cl_2 (2.5:1.5 v/v).

halogenated BODIPYs, which can be efficiently synthesized from dipyrrylketones.[29]

Steady-State UV–vis Absorption and Fluorescence Spectroscopy of 1 in Organic Solvents. The UV–vis absorption and fluorescence emission spectra of **1** in a selection of organic solvents are shown in Figure 2. BODIPY derivative **1** displays several unusual spectroscopic properties in relation to unsubstituted BODIPY and classic boradiazaindacene dyes.[2−5] The most striking property of **1** is the clearly blue-shifted absorption and emission spectra with respect to unsubstituted and other common BODIPY derivatives. Table 1 compiles the spectroscopic and photophysical data of **1** as a function of solvent.

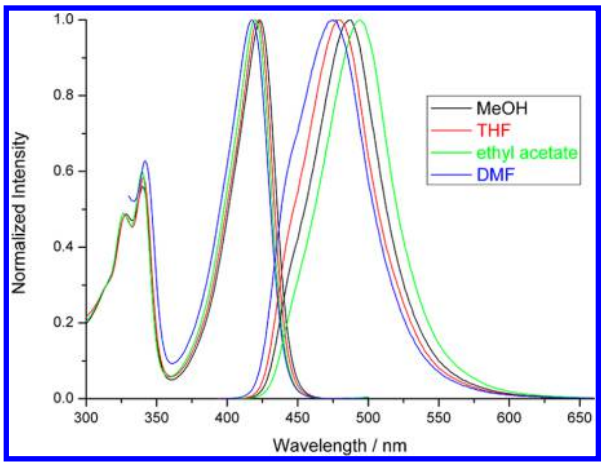

Figure 2. Normalized absorption and fluorescence emission spectra (upon excitation at 390 nm) of **1** in the solvents indicated. Measurements were performed at room temperature.

The main absorption band of **1** with the maximum λ_{abs}(max) positioned in the range from 415 nm (in acetonitrile and acetone) to 429 nm (in cyclohexane and toluene) is assigned to the $S_1 \leftarrow S_0$ transition. An additional, weaker absorption band can be observed in the UV region from 320 to 330 nm and is attributed to the $S_2 \leftarrow S_0$ transition. In ethanol, the molar absorption coefficient ε_{max} [at λ_{abs}(max) = 424 nm] is (36.1 ± 0.8) × 10^3 L mol^{-1} cm^{-1}. The corresponding molecular brightness is 29 600 L mol^{-1} cm^{-1} [as obtained by the product $\varepsilon(\lambda_{abs})\Phi$ with Φ being the fluorescence quantum yield (Table 1)],[30] demonstrating that **1** is a bright fluorophore. Table 1 shows that the absorption ($fwhm_{abs}$) and emission ($fwhm_{em}$) bandwidths (full width at half-maximum) of **1** are significantly wider than those of typical BODIPYs.[2−5] Blue-shifted λ_{abs}(max) and λ_{em}(max) and broader bandwidths $fwhm_{abs}$ and $fwhm_{em}$ in relation to those of classic difluoroboron dipyrrins have been observed for other *meso*-amino substituted BODIPYs.[24−28,31] The $fwhm_{em}$ of **1** are consistently larger than the $fwhm_{abs}$ (Table 1), which could suggest a decreased rigidity in the excited state compared to the ground state.

Probe **1** shows a Stokes-shifted emission band, which mirrors the absorption band in shape. Its maximum λ_{em}(max) is shifted from 474 nm (in acetone) to 494 nm (in acetic acid). In all solvents tested, the fluorescence excitation spectra of **1** match the corresponding absorption spectra. The Stokes shifts $\Delta\bar{\nu}$ of **1** are considerably larger than those of unsubstituted and common difluoroboron dipyrrins[2−5] (Table 1). This is in agreement with earlier observations for 8-aminoBODIPYs.[24−28,31] The $\Delta\bar{\nu}$ value averaged over the 12 solvents (see Table 1) equals 2967 ± 154 cm^{-1}. The fluorescence quantum yields Φ are moderate to high (between 0.38 and 0.93), the lowest value being observed in polar DMSO.

Table 1. Spectroscopic and Photophysical Data of 1 as a Function of Solvent[a]

nr	solvent	λ_{abs}(max)[b] [nm]	λ_{em}(max)[c] [nm]	$\Delta\bar{\nu}$[d] [cm^{-1}]	$fwhm_{abs}$[e] [cm^{-1}]	$fwhm_{em}$[f] [cm^{-1}]	Φ[g]	τ[h] [ns]	k_f[i] [10^8 s^{-1}]	k_{nr}[i] [10^8 s^{-1}]
1	methanol	423	487	3107	1984	2485	0.81 ± 0.02	4.43 ± 0.05	1.83 ± 0.05	0.43 ± 0.06
2	acetonitile	415	477	3132	2164	2771	0.71 ± 0.02	3.78 ± 0.04	1.88 ± 0.06	0.77 ± 0.06
3	acetone	415	474	2999	2081	2930	0.69 ± 0.01	3.38 ± 0.04	2.04 ± 0.04	0.92 ± 0.05
4	ethanol	424	485	2966	1940	2538	0.82 ± 0.05	4.16 ± 0.05	1.97 ± 0.12	0.43 ± 0.13
5	acetic acid	425	494	3287	2044	2412	0.81 ± 0.04	4.47 ± 0.05	1.81 ± 0.09	0.43 ± 0.10
6	ethyl acetate	420	480	2976	1977	2609	0.81 ± 0.01	3.61 ± 0.04	2.23 ± 0.04	0.54 ± 0.05
7	2-propanol	424	483	2881	1887	2563	0.93 ± 0.01	4.02 ± 0.05	2.31 ± 0.04	0.18 ± 0.05
8	THF	422	480	2863	2032	2647	0.79 ± 0.01	3.77 ± 0.04[j]	2.10 ± 0.03	0.56 ± 0.04
9	cyclohexane	429	487	2776	2504	4374	0.62 ± 0.02	4.00 ± 0.05	1.54 ± 0.04	0.96 ± 0.05
10	DMF	417	476	2972	2105	2977	0.52 ± 0.01	2.62 ± 0.03	2.00 ± 0.04	1.82 ± 0.06
11	DMSO	418	476	2915	2115	2995	0.38 ± 0.01	1.59 ± 0.02	2.36 ± 0.04	3.92 ± 0.09
12	toluene	429	486	2734	2247	3786	0.58 ± 0.01	3.31 ± 0.05	1.74 ± 0.04	1.28 ± 0.06

[a]The solvents are ranked according to increasing refractive index *n*. [b]Wavelength of absorption maximum. [c]Wavelength of fluorescence emission maximum. [d]Stokes shift [$\Delta\bar{\nu} = 1/\lambda_{abs}(max) - 1/\lambda_{em}(max)$]. [e]Full width at half-height of the maximum of the absorption band. [f]Full width at half-height of the maximum of the fluorescence emission band. [g]Fluorescence quantum yield ± one standard uncertainty. Φ determined versus coumarin 1 in ethanol (Φ_r = 0.64) as reference. [h]Excitation wavelength = 342 nm (one-photon excitation using single-photon timing technique), except for THF (see *j*, two-photon excitation using FLIM technique). The uncertainties represent the standard deviation. [i]Rate constants of deactivation of the singlet excited state via fluorescence (k_f) and nonradiative processes (k_{nr}). The propagated errors are calculated using the standard uncertainty of Φ and the standard error of τ. [j]Excitation wavelength = 840 nm (two-photon excitation using FLIM technique).

DOI: 10.1021/acs.langmuir.6b00478
Langmuir 2016, 32, 3495−3505

The solvent only slightly influences the spectral maxima $\lambda_{abs}(max)$ and $\lambda_{em}(max)$ of **1** (Table 1 and Figure 2). Indeed, $\lambda_{abs}(max)$ varies by 14 nm (786 cm^{-1}) among the 12 solvents tested, and $\lambda_{em}(max)$ varies by 20 nm (854 cm^{-1}). It is worthwhile to rationalize these modest but significant solvent-dependent shifts. The most recent, comprehensive treatment of the solvent effect (based on a set of four empirical, complementary, mutually independent solvent scales, that is, dipolarity, polarizability, acidity, and basicity of the medium) has been proposed by Catalán.[32] In this method, the polarizability and dipolarity of a particular solvent are characterized by the parameters SP and SdP, respectively, whereas acidity and basicity are described by the scales SA and SB, respectively. The {SA, SB, SP, SdP} parameters for a large number of solvents can be found in ref 32. Mathematically, the solvent effect on the physicochemical observable y can be expressed by the multilinear eq 1

$$y = y_0 + a_{SA}SA + b_{SB}SB + c_{SP}SP + d_{SdP}SdP \quad (1)$$

where y_0 denotes the physicochemical property of interest in the gas phase; a_{SA}, b_{SB}, c_{SP}, and d_{SdP} are regression coefficients that describe the sensitivity of the property y to the various solvent−solute interaction mechanisms; and {SA, SB, SP, SdP} are independent solvent parameters (indices) accounting for the various types of solvent−solute interactions.

The spectroscopic observables y analyzed in this paper are the absorption maxima $\bar{\nu}_{abs} = 1/\lambda_{abs}(max)$ and the emission maxima $\bar{\nu}_{em} = 1/\lambda_{em}(max)$, both expressed in cm^{-1}.

The use of {SA, SB, SP, SdP} (eq 1) gives high-quality fits to $\bar{\nu}_{abs}$ of **1**, using the correlation coefficient r as goodness-of-fit criterion (r = 0.964, eq 2 with 12 data points, uncertainties on the coefficients are standard errors)

$$\bar{\nu}_{abs} = (23859 \pm 332) - (609 \pm 128)SA - (327 \pm 169)SB - (838 \pm 459)SP + (977 \pm 124)SdP \quad (2)$$

High-quality fits are also obtained for the multilinear analysis (eq 1) of $\bar{\nu}_{em}$ (r = 0.987, eq 3 with 12 data points, uncertainties on the coefficients are standard errors as calculated from the covariance matrix resulting from the analysis)

$$\bar{\nu}_{em} = (20683 \pm 187) - (904 \pm 72)SA + (47 \pm 95)SB - (299 \pm 258)SP + (570 \pm 70)SdP \quad (3)$$

The added benefit of the generalized (Catalán) treatment of the solvent effect is that it allows the separation of the relative contributions of dipolarity, polarizability, acidity, and basicity of the medium. Therefore, we utilized the new methodology to resolve which solvent property/properties is/are primarily responsible for the observed shifts of $\bar{\nu}_{abs}$ and $\bar{\nu}_{em}$. The relative importance of each of the Catalán solvent parameters was studied by omitting each solvent scale in turn in the regression analysis.

SA and SdP exhibit major contributions (i.e., large a_{SA} and d_{SdP} values) with small, relative standard errors in eq 2, which is further cross-checked by the excellent fits obtained when both SA and SdP are present in the analyses (i.e., for sets {SA, SB, SdP} and {SA, SP, SdP} with r = 0.947 and 0.945, respectively). This indicates that solvent acidity and dipolarity are crucial for $\bar{\nu}_{abs}$. Conversely, when either SA or SdP is omitted from the regression analysis, the fit becomes unacceptable with r-values of 0.838 and 0.554 for sets {SB, SP, SdP} and {SA, SB, SP}, respectively. The crucial role of solvent acidity and dipolarity is additionally evidenced by the high r-value (0.927) obtained with the {SA, SdP} set. That solvent basicity and polarizability play no role is evident from the analysis with {SB, SP}, yielding a r-value of only 0.376. The negligible influence of solvent polarizability on $\bar{\nu}_{abs}$ is further corroborated by the weak linear correlation between $\bar{\nu}_{abs}$ and the Bayliss function $f(n) = (n^2 - 1)/(2n^2 + 1)$ (r = −0.298).

Similar results are obtained for $\bar{\nu}_{em}$. The large estimated a_{SA} and d_{SdP} values and their relatively small standard errors in eq 3 are an indication that the change of $\bar{\nu}_{em}$ may reflect predominantly a variation of acidity and dipolarity of the environment of the chromophore. This is backed up by the analyses in which either SA or SdP is omitted from eq 1. Indeed, the r-values are significantly lowered for sets {SB, SP, SdP} (r = 0.635) and {SA, SB, SP} (r = 0.856), compared to 0.987, as found for eq 3. Conversely, as long as SA and SdP are simultaneously present in the analysis, high-quality fits are obtained (i.e., for sets {SA, SB, SdP} and {SA, SP, SdP} with r = 0.985 and 0.987, respectively). This demonstrates the crucial role of solvent acidity and dipolarity to rationalize the solvent-dependent location of $\bar{\nu}_{em}$. Additionally, the multilinear regression of $\bar{\nu}_{em}$ according to eq 1 with only {SA, SdP} as independent variables yielded an excellent fit with a high r-value (0.984), very close to that of the original fit (eq 3, r = 0.987). Once more, solvent basicity and polarizability have an insignificant effect on the position of $\bar{\nu}_{em}$, as evidenced by the analysis with {SB, SP}, yielding a r-value of only 0.470. Extra confirmation that solvent polarizability is an unimportant parameter affecting $\bar{\nu}_{em}$ comes from the poor linear correlation between $\bar{\nu}_{em}$ and the Bayliss function $f(n)$ (r = 0.091).

Time-Resolved Fluorescence. The fluorescence decays obtained by SPT by one-photon excitation were performed at 342 nm using samples of **1** in quartz cuvettes. To determine the appropriate excitation wavelength for the two-photon excitation, excitation finger printing was performed for different solvents. The highest intensity observed for **1** dissolved in methanol was at 840 nm (Figure S1, Supporting Information). FLIM experiments were conducted with two-photon excitation at 840 nm using samples of **1** on the microscope stage. The fluorescence decay curves were found to be monoexponential [$f(t) = \alpha \exp(-t/\tau)$]. The fluorescence (nanosecond) lifetimes τ obtained by both SPT and FLIM are equal (Table 2). Using the experimental fluorescence quantum yield (Φ) and the monoexponential lifetime (τ), the rate constants of radiative ($k_f = \Phi_f/\tau$) and nonradiative [$k_{nr} = (1 - \Phi_f)/\tau$] decay (Table 1) were calculated. The average k_f value ±1 standard uncertainty is

Table 2. Fluorescence Lifetimes τ Obtained upon One-Photon (342 and 420 nm) and Two-Photon Excitation (840 nm)[a]

solvent	τ [ns] (one-photon excitation)	τ [ns] (two-photon excitation)
DMSO	1.70 ± 0.01[b]	1.71 ± 0.06[c]
ethanol	4.16 ± 0.05[b]	4.22 ± 0.05[c]
ethanol	4.20 ± 0.20[d]	4.20 ± 0.40[e]
methanol	4.43 ± 0.05[b]	4.39 ± 0.07[c]

[a]The quoted uncertainties represent the standard deviation. [b]λ_{ex} = 342 nm, single-photon timing. [c]λ_{ex} = 840 nm, FLIM. [d]λ_{ex} = 420 nm, fluorescence up-conversion. [e]λ_{ex} = 840 nm, fluorescence up-conversion.

DOI: 10.1021/acs.langmuir.6b00478
Langmuir 2016, 32, 3495−3505

$(2.0 \pm 0.2) \times 10^8$ s^{-1}, which is somewhat higher than the k_f values commonly found for classic BODIPY dyes (i.e., in the range from 1.4 to 1.7 $\times$ 10^8 s^{-1}).[2−5] The solvent-dependent observations made for k_f were also valid for k_{nr}; there is no systematic solvent dependency of k_{nr}. The average k_{nr} value ±1 standard uncertainty for the solvents of Table 1 is $(1.0 \pm 1.0) \times 10^8$ s^{-1}.

The excited-state properties of **1** in ethanol were further investigated in a series of time-resolved fluorescence experiments using the up-conversion technique with femtosecond time resolution. Fluorescence decays were recorded close to λ_{em}(max) (490 nm) in two time windows (50 and 420 ps) with the excitation wavelength set at 420 nm. In order to investigate the two-photon excitation intrinsic properties of **1** and to observe the dynamics of its excited-state, an additional set of experiments were performed with an 840 nm excitation wavelength while maintaining the detection at 490 nm.

The analysis of the time-resolved fluorescence traces obtained upon 420 nm excitation revealed three decay times of 4.8, 47, and 4200 ps (Figures S2 and S3, Supporting Information) with only the latter having a positive pre-exponential factor. Although **1** exhibits a clear fluorescence emission upon two-photon excitation in ethanol (Figures S4 and S5, Supporting Information), the signal-to-noise ratio is low as a result of two effects: the high intensity beam impinging on the sample generates photobleaching and white light generation (note the high intensity signal at the excitation time). The kinetic fluorescence trace profile appears similar to that observed for the one-photon excitation process (Figures S2 and S3, Supporting Information). Such kinetic similarities suggest that, following the Franck−Condon excitation, the fluorescence emission occurs from an excited state with similar spectroscopic characteristics as the one observed upon one-photon 420 nm excitation.

Fluorescence Properties of 1 in Small Unilamellar Vesicles. The fluorescence properties of **1** were determined in small unilamellar vesicles (SUV), a widely used lipid model system. The fluorescence excitation and emission spectra of **1** (Figure S6, Supporting Information) were recorded at room temperature so that the various lipid systems exhibit different lipid phases, that is, liquid disordered phase (L_d) for DOPC and gel phase (S_o) for both DPPC and DSPC.

The excitation spectra of **1** were found to be similar in the various lipid systems with almost no change of λ_{ex}(max) (Table 3). The emission spectra of **1** exhibit a small bathochromic shift (11 nm) of the L_d phase in relation to the S_o phase. A similar shift is observed upon increasing the temperature of the DPPC or DSPC SUV lipid system (Figure S7, Supporting Information). The spectra of **1** are not influenced by the length of the aliphatic SUV lipid chains, as shown by the similar emission spectra in DPPC and DSPC SUVs (Figure S7, Supporting Information).

Table 3. Excitation [λ_{ex}(max)] and Emission [λ_{em}(max)] Maxima and Fluorescence Lifetimes τ of 1 Inserted in SUVs with Different Composition at Room Temperature

	DOPC (L_d)	DPPC (S_o)	DSPC (S_o)
λ_{ex}(max) [nm]	421	420	419
λ_{em}(max) [nm]	484	477	473
τ [ns][a]	4.3 ± 0.1	4.3 ± 0.1	4.4 ± 0.2

[a]The uncertainties represent the standard deviation.

Fluorescence anisotropy of **1** in DPPC and DSPC SUVs was recorded at 472 nm with the excitation set at 420 nm and at temperatures between 10 and 70 °C (Figure S8, Supporting Information). The fluorescence anisotropy is high in the S_o phase and decreases with increasing temperature and lipid membrane fluidity. The temperature dependence was fitted with a sigmoidal function and the transition temperature (T_m) of the lipids was given by the inflection point, 39.1 ± 0.5 °C for DPPC and 51.9 ± 0.7 °C for DSPC. These values are close to those reported in the literature for SUVs (37.8 ± 1.0 °C for DPPC and 51.8 ± 1.1 °C for DSPC).[33]

Fluorescence decay measurements under single-photon excitation were performed on the SUVs with a single type of phospholipid (DOPC, DPPC, DSPC) (Table 3). The decay traces were well fitted with a single-exponential and the fluorescence lifetime is essentially independent of the lipid phase. For DPPC and DSPC SUVs, the fluorescence lifetimes were measured at various temperatures and no temperature dependence was observed (Table S1).

Discrimination of Lipid Phases by 1 in Giant Unilamellar Vesicles. To study the spatial distribution of **1** over different lipid phases, experiments were performed on giant unilamellar vesicles (GUVs). The distribution of **1** over four different lipid phases (S_o, L_d, L_d/S_o, and L_o/L_d) was investigated by confocal laser scanning microscopy (CLSM) at room temperature. The GUVs had different compositions, DPPC, DOPC, DOPC/DPPC (4:6 molar ratio), and DOPC/SM/Chol (1:2:1 molar ratio). Apart from photoselection effects, a uniform distribution is observed for **1** in the L_d and S_o systems (Figure S9, Supporting Information).

The GUVs of mixed composition were loaded simultaneously with both **1** and DiI-C_{18}(5) to assign the type of lipid phase. DiI-C_{18}(5) and DiI-C_{18}(3) have similar membrane properties[23] and both probes partition preferentially in the S_o phase for DOPC/DPPC mixtures[34,35] and tentatively in the L_d phase for DOPC/SM/Chol mixtures that exhibit phase separation.[22,23,36] We observed that DiI-C_{18}(5) and **1** accumulate preferentially in the same phase in both the DOPC/DPPC mixture (Figure S10A,B) and the DOPC/SM/Chol mixture (Figure S10C,D).

To observe the shape of the lipid phases, we recorded *z*-stacks of the GUVs from the two mixed systems with steps of 0.5 or 1 μm (Figure 3). DOPC-rich domains representing the L_d phase for the DOPC/SM/Chol mixture[22,35] can be observed in Figure 3A. The stripe and patch domains that are typical for the S_o phase of the DOPC/DPPC mixture[34,35] are shown in Figure 3B.

Fluorescence lifetime images were also recorded for each type of GUV and the lifetime distributions for each of the phases are shown in Figure S11 (Supporting Information). An average lifetime was calculated for each phase within the GUV and averaged over at least 10 GUVs (Table 4). Except for the values obtained for the solid phase of the DOPC/DPPC mixture, no significant differences were observed between the various lipid phases.

FRAP measurements were performed at room temperature on GUVs stained with **1** prepared from either DOPC or DPPC. In both cases, the mobile fraction was close to 100%. In the gel phase (DPPC), the average value for the diffusion coefficient *D* equals 0.13 ± 0.02 $\mu m^2/s$, whereas for the fluid phase the increase of mobility leads to a substantially higher value, namely $D = 4 \pm 2$ $\mu m^2/s$ in DOPC. The high uncertainty for DOPC GUVs arises from the limited temporal resolution of the

DOI: 10.1021/acs.langmuir.6b00478
Langmuir 2016, 32, 3495−3505

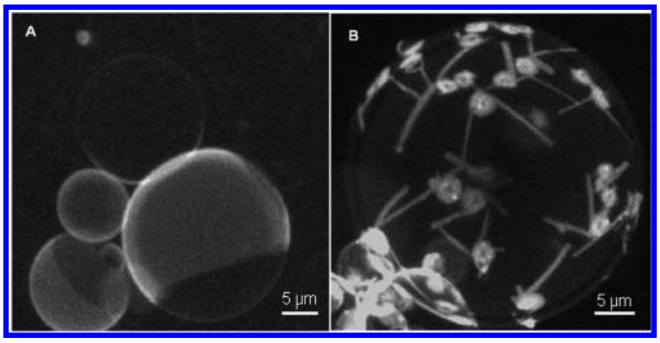

Figure 3. Intensity image of GUVs obtained for probe **1** by superimposing the images from a *z*-stack. Panel A shows the L_o/L_d phase separation (DOPC/SM/Chol) and panel B displays the L_d/S_o phase mixture (DOPC/DPPC). Depending on the relative position and size of the GUVs, different intensities for different areas can result from the superposition of the images in the z-stack. Measurements were performed at room temperature. The excitation light (840 nm) was linearly polarized along the horizontal axis.

microscope used in the FRAP experiment. Therefore, additional RICS measurements were performed to accurately measure the diffusion coefficient D of **1** in DOPC, yielding a D value of 4.5 ± 0.8 $\mu m^2/s$ (Figure S12, Supporting Information).

Location and Orientation of 1 in the DOPC Lipid Membrane by Molecular Dynamics. Molecular dynamics (MD) simulations have repeatedly been shown to provide positioning of small molecules in DOPC bilayers in agreement with experimental data.[37−42] Here, the equilibrated geometries obtained after MD simulations considering a temperature of 310 K indicate that **1** systematically incorporates into the DOPC bilayer regardless of its initial location and orientation. As can be seen in Figure S13 (Supporting Information), the location is equilibrated after 40 ns. Therefore, all geometrical observables (distances and angles) are averaged from 40 to 300 ns. These calculations indicate that **1** is located below the membrane surface in zones 2−4 (Figure 4). The long octadecyl chains of **1** are located in zones 3−4, that is, the hydrophobic core of the bilayer. The boron atom of the BODIPY chromophore lies in zone 2 (the high headgroup density region, Figure 4) at 1.2 nm from the center of the membrane or 0.8 nm below the phosphorus atoms of the membrane surface. As expected, the sulfonate moiety is embedded in this region close to zone 1, which tightly anchors the probe (the standard deviation of the location is ca. 0.2 nm).

The averaged orientation of **1** is characterized by the α_1-angle between the normal to the plane of the π-conjugated core and the *z*-axis (perpendicular to the bilayer surface). Taking fluctuations at 298 K into consideration, this angle is in the range from 50 to 160° with one well-defined maximum at 117° in its distribution (Figure S14, Supporting Information). This maximum describes the π-conjugated core as being slightly deviated from the perpendicular orientation with respect to the membrane surface. This is attributed to the flexibility of the CH_2CH_2 chain linking the SO_3^- and NH groups of the taurine *meso*-substituent. To fully characterize the orientation of the fluorescent moiety in the DOPC bilayer, the α_2-angle between the longest axis of the π-conjugated core and the *z*-axis was also considered. The absorption transition dipole moment of **1** is oriented along the long axis of the π-conjugated core (Figure 4), as confirmed by a single-point quantum-chemical calculation upon the ground-state geometry of **1** using time-dependent density functional theory (TDDFT) along with the hybrid BHLYP functional and the DZP basis set. Calculations indicated that both the transition dipole moments of absorption and emission are parallel.

The α_2-angle fluctuates in a broad range with an average value of 70° (Figure S15, Supporting Information), showing that the transition dipole moment is slightly off from the perpendicular orientation with respect to the *z*-axis, that is, parallel orientation with respect to the surface.

Fluorescence Measurements in Biological Cells. CLSM measurements were performed on live OLN-93 cells at room temperature. These cells were selected because they exhibit membrane inhomogeneities in lipid organization.[44] The dye accumulates both in the plasma membrane and cytoplasm but remains excluded from the nucleus (Figure S16, Supporting Information). No segregation of **1** within the cell membrane was observed.

In contrast to the pure, organic solvents where the fluorescence decays were well fitted with a single exponential, the decays in the cells required two exponentials to reach an acceptable fit, both for the cell membrane and for the cytosol (Figure 5). The shorter decay time is between 0.2 and 0.4 ns in the membrane and between 0.2 and 0.6 ns in the cytosol, whereas the longer one is between 2 and 3.5 ns in the membrane and between 2 and 4 ns in the cytosol. The pre-exponentials of the two decay times vary between membrane and cytosol, that is, the ratio of the longer decay time over the shorter one is lower in the cytosol as compared with the ratio obtained for the membrane.

The translational mobility of **1** in the membrane of OLN-93 cells was studied using FRAP. The weighted average based on the standard deviation of the diffusion constant D from five measurements is 0.18 ± 0.02 $\mu m^2/s$ (values are between 0.08 and 0.48), whereas the mobile fraction is 91 ± 1% (Figure S12, Supporting Information).

■ DISCUSSION

The new probe **1** described in this work represents the first blue-emitting BODIPY-based lipid probe, whereas currently available BODIPY lipid probes are characterized by a yellow-red emission. 8-AminoBODIPYs, of which compound **1** is an example, are characterized by fluorescence in the blue spectral region, which is unusual for difluoroboron dipyrrins.[24−28,31]

The solvatochromic analysis of **1** in pure solvents indicates that the absorption and emission maxima are determined

Table 4. Average Fluorescence Lifetimes τ (in ns) of 1 Obtained for the Different Lipid Phases in the Various Types of GUVs at Room Temperature

DOPC	DOPC/SM/Chol		DOPC/DPPC		DPPC
L_d	L_o	L_d	L_d	S_o	S_o
4.3 ± 0.1[a]	4.5 ± 0.2	4.4 ± 0.2	4.1 ± 0.2	4.0 ± 0.2	4.2 ± 0.2

[a]The uncertainties represent the standard deviation.

DOI: 10.1021/acs.langmuir.6b00478
Langmuir 2016, 32, 3495−3505

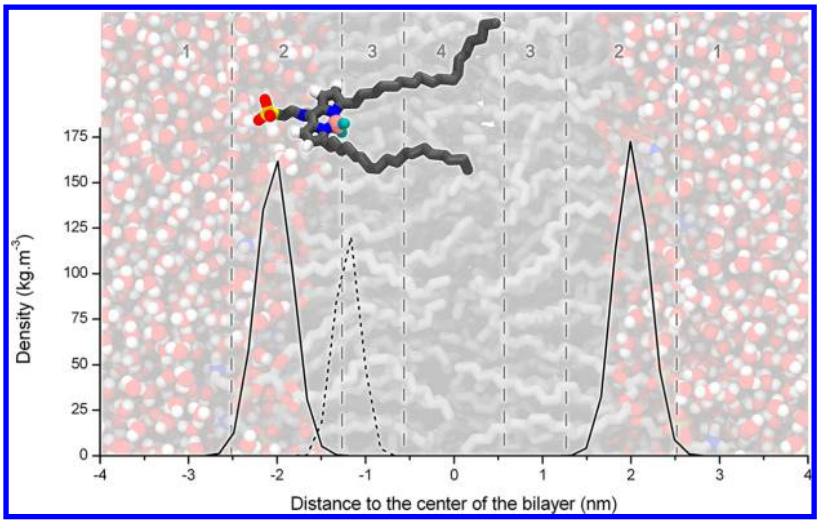

Figure 4. Normalized partial densities of the phosphorus atoms in the upper- and under-layer of the membrane (full line) and of the boron atom of the BODIPY core (dashed line) in DOPC considering a temperature of 310 K. The results are averaged along the MD simulation in the range from 40 to 300 ns. The picture is a representative snapshot of **1** within the DOPC bilayer. In the foreground, the probe is depicted together with its first transition state dipole moment (in green). The lipid chains are given in gray, as well as the carbon backbone of the BODIPY core. The color coding of specific atoms is as follows: boron (pink), fluor (light blue), nitrogen (dark blue), sulfur (yellow), and oxygen (red); as the united atom model is used, only the hydrogen atoms in an sp^2 hybridization (in white) are indicated in the probe. The vertical dashed lines indicate the boundaries between the different regions of (1) low headgroup density, (2) high headgroup density, (3) high tail density, and (4) low tail density, as defined by the classification of Marrink and Berendsen.[43]

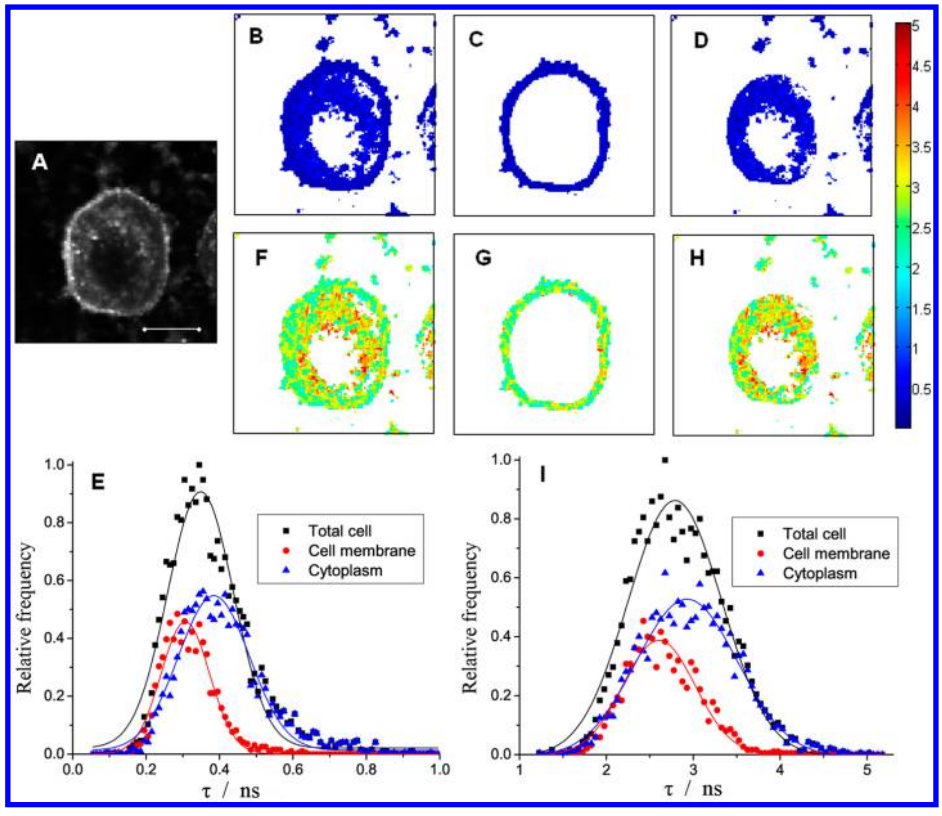

Figure 5. Intensity image of **1** in OLN-93 cells (A). FLIM images of the entire OLN-93 cell (B,F), the plasma membrane (C,G) and the cytosol (D,H). Decay time distribution of the shorter (E) and longer (I) decay times recorded in the cells. Measurements were performed at room temperature. Excitation light was set at 840 nm and was linearly polarized along the horizontal axis. The size of the scale bar is 10 μm for all the images.

mainly by solvent acidity and dipolarity, and that solvent basicity and polarizability play no role. In this respect, compound **1** differs quite strongly from most BODIPYs investigated earlier where solvent polarizability was the major cause for the solvent dependence of $\bar{\nu}_{abs}$.[5] The lack of effect of solvent polarizability on $\bar{\nu}_{abs}$ and $\bar{\nu}_{em}$ contrasts with earlier reports on common BODIPY dyes[5] where polarizability is the primary factor responsible for the small solvent-dependent

DOI: 10.1021/acs.langmuir.6b00478
Langmuir 2016, 32, 3495−3505

shifts of the visible absorption and fluorescence emission bands of these dyes. This is in line with quantum chemical density functional theory calculations, which show an increased HOMO−LUMO band gap compared to common BODIPY dyes. These calculations also support the observed hypsochromic spectral shifts, which are found to be due to a net destabilization of the LUMO state whereas the HOMO energy remains unaltered by the presence of a *meso*-amino group.[25,27,28,31] This illustrates once more that **1** has quite unusual properties compared to already described 8-amino-BODIPYs.[24−28,31]

The fluorescence quantum yield is high in the various solvents investigated. The fluorescence lifetime depends on the solvent but is the same irrespective of excitation at 342 or 420 nm in 1-photon or at 840 nm in 2-photon mode. The up-conversion approach revealed three components in the fluorescence relaxation of **1** in ethanol. The slow component (4.2 ns) with positive amplitude found back in SPT experiments can be attributed directly to the decay of the relaxed S_1 state. Interestingly, the fast components of 4.8 and 47 ps have negative contributions (rise components) and could indicate the presence of significant vibrational and/or structural relaxation processes occurring in the excited state of the chromophore. This could also account for the large Stokes shift $\Delta\bar{\nu}$ (~3000 cm^{-1}) in the steady-state data (Table 1) in relation to those observed for other classic BODIPY dyes.[2−5]

The fluorescence decay of **1** is monoexponential in SUVs and GUVs. The lifetime is independent of the type and the phase of the lipid and resembles that of **1** in ethanol and methanol, that is, somewhat more than 4 ns. The fluorescence relaxation of **1** in the more complex environment of the plasma membrane and the cytosol of OLN-93 cells can be described by a sum of two exponentially decaying functions. The two relaxation times associated with the plasma membrane are somewhat shorter than the two relaxation times in the cytosol. The interpretation of the relaxation times in the biological cell is difficult and is beyond the scope of this study. Also the fluorescence decay of carbocyanine dyes in artificial lipid system comprises two components and the average lifetime is ca. 1 ns and depends on the lipid phase.[45]

Probe **1** is well anchored into the lipid membrane due to the C_{18}-alkyl chains as well as the boron atom. The MD calculations indicate that the fluorescent moiety is clearly located below the polar head region. Similar observations have been obtained with MD for DiI-C_{18}(3).[39] The BODIPY core of **1** resides at 1.2 nm from the center of the membrane, whereas the chromophore of DiI-C_{18}(3) was at 1.26 nm from the center. Our MD calculations revealed an average value of 70° between the transition dipole moment of **1** and the normal to the DOPC lipid membrane at 310 K. This compares very well with the value reported for the average orientation of the long axis of the DiI-C_{18}(3) chromophore that is 77° in DPPC above the phase temperature.[39] For both dyes, the angular distributions are rather broad. This rationalizes our observation that the photoselection effect is not as strong as could be expected for a cross-section through the GUVs.

The position of **1**, determined by hydrophobic tails and a hydrophilic headgroup, follows the analysis based upon solvent acidity and dipolarity. The equilibrium positions and the distance of the core moiety of **1** to the center of the membrane are therefore found to be very similar in simulations performed in DOPC as well as DPPC tissues in the Ld phase. For DPPC in the S_o phase, the distance to the membrane surface is decreased [work in progress]. The lower packing coefficient in the L_d phase allows for an enhanced solvation and brings along stronger hydrophobic effects, causing the tails to penetrate deeper into the membrane. These effects are also responsible for the shift of the emission spectra as a function of temperature (see Figure S7). Microscopy measurements performed on GUVs with mixed lipid compositions established that the probe partitions preferentially into the same lipid phase as DiI-C_{18}(5).

A high steady-state fluorescence anisotropy of **1** was found in the S_o phase. Similar observations were reported for carbocyanine dyes.[46,47] The fluorescence anisotropy of **1** decreases upon transition to a more fluidlike lipid environment. Indeed, with an obtained angle difference of barely 6.0° between the absorption and emission dipole moments of **1** our MD calculations for the DOPC in the L_d phase indicate that these vectors are nearly parallel. As the fluorescence lifetime is essentially independent of both lipid phase and temperature of the artificial lipid system, the interpretation of steady-state fluorescence anisotropy experiments is rather straightforward. Changes in fluorescence anisotropy are then entirely due to wobbling motions of the probe. As the lifetime of **1** is larger than the lifetime of DiI-C18(5), the steady state fluorescence anisotropy of **1** is more sensitive to slower rotational motions of the dye. MD calculations for DiI-C_{18}(3) have demonstrated that free volumes exist in the region just beneath the water−headgroup interface allowing for such wobbling motions of the transition moment.[39] Depolarization can also occur by rotation of the molecule as whole but at a slower rate. This suggests that, as for DiI-C_{18}(3),[39] the time-resolved anisotropy decay of **1** will comprise two relaxation times and a limiting anisotropy at long times because of the restricted wobbling motions.[48,49] The length of the lipid chains does not influence the behavior of **1**, because the fluorescence anisotropy values obtained for C_{16} and C_{18} lipid systems were similar when being in the same phase.

Recently, Timr et al.[50] investigated the two-photon absorption of DiI(3) by reverting to a sum-overstates expression and a diagonalization of the two-photon transition tensor. The latter was found to be dominated by the transition dipole moment and the change between the ground and first excited state dipole moments, which are perpendicular to each other for the DiI species. Because the orientation of these two vectors is found to be analogous for **1**, it can be expected that also for **1** the one-photon optical anisotropy properties cannot be used to estimate anisotropy properties of two-photon absorption.[50]

Lateral diffusion measurements of **1** were performed both in GUVs and OLN-93 cells. Diffusion coefficients obtained for the gel (0.13 ± 0.02 $\mu m^2/s$) and fluid (4.5 ± 0.8 $\mu m^2/s$) phase of the GUVs differ by 1 order of magnitude. Gielen et al.[51] reported that the diffusion coefficients of DiI-C_{18}(5) inserted in POPC GUVs (fluid phase) are around 7 $\mu m^2/s$. Similar values were also found for DiI-C_{18}(3) in DOPC GUVs (fluid phase).[19,22] FRAP measurements performed on DiI-C_{18}(5) in primary oligodendrocytes derived from neonatal rat brains yielded diffusion coefficient values ranging from 0.4 to 2.8 $\mu m^2/s$,[51] which are somewhat higher compared with those obtained here for **1** in OLN-93 (with values ranging from 0.08 to 0.48 $\mu m^2/s$). As reported previously, the diffusion coefficients of fluorescent probes in the plasma membrane are slower than those recorded in model membranes.[52] Given the similar behavior of the membrane probes **1** and DiI-C_{18}(5), **1** can be seen as a promising alternative to DiI-C_{18} type probes in the

DOI: 10.1021/acs.langmuir.6b00478
Langmuir 2016, 32, 3495−3505

blue spectral region. Considering the excitation/emission spectra of **1**, its transition dipole orientation, and phase partitioning similar to other fluorescent probes (i.e., some of the DiI and DiO probes[53−56]), the new BODIPY-based probe appears particularly adapted for Förster resonance energy transfer studies in lipid bilayers.

CONCLUSIONS

Lipid membranes exhibit various phases and characteristics depending on their composition and temperature. Cholesterol and its relative abundance are found to play a major role in the formation of so-called lipid rafts, which are expected to result from their interaction with long saturated alkyl chain lipids like, for example, sphingomyelin. In view of the dynamic and fragile nature of the rafts, optical methods making use of suitable probes are of paramount interest, as they can both provide information on the structure and the dynamics of molecular biosystems within high temporal and spatial boundaries. The spatial heterogeneity of the membrane properties influences the membrane protein distribution, which in turn has consequences for the cell physiology.

Currently, membrane probes of the dialkyl carbocyanine (DiI) family are widely used because they take a well-defined position within the membrane and are known to be able to selectively partition into particular phases of the membrane. However, these DiI probes are exclusively used in relation with low-energy orange light.

In this work, we describe the new BODIPY-based membrane probe 1. This lipid probe 1 has been found to exhibit three key characteristics, which were prerequisites for its development: (i) it has been found to be excitable in the blue spectral region by both 1- and 2-photons in combination with a high fluorescence quantum yield; (ii) it partitions preferentially in the same lipid phase as DiI-C18(5) of the DiI family; and (iii) its transition dipole moment is almost parallel to the membrane surface, thus allowing for the observation of lipid membranes at orientations perpendicular to the excitation beam. Therefore, it can be concluded that **1** is a valid alternative to the DiI-C18(5) probe if excitation in the blue region of the spectrum is required. This allows for new combinations of dyes in the exploration of membrane properties and the spatial distribution of membrane associated proteins. As the length of the hydrocarbon chains of **1** can easily be adapted, new approaches within the area of membrane analysis of lipid membrane related aspects, fluorescence microscopy, and bioimaging in general become possible.

ASSOCIATED CONTENT

Supporting Information

The Supporting Information is available free of charge on the ACS Publications website at DOI: 10.1021/acs.langmuir.6b00478.

Detailed synthesis of **1** and determination of fluorescence quantum yield. Experimental section. Two-photon excitation fingerprinting of **1**. Fluorescence up-conversion and the fluorescence decay traces recorded. Photophysical parameters of **1** in SUVs and GUVs. Diffusion measurements using FRAP and RICS at room temperature in GUVs and OLN-93 cells. MD calculations. OLN-93 cells stained with **1**.
(PDF)

AUTHOR INFORMATION

Corresponding Author

*E-mail: marcel.ameloot@uhasselt.be. Tel: +32-11-269233. Fax: +32-11-269299.

Present Addresses

◆(L.W.) College of Environment and Safety Engineering, Qingdao University of Science and Technology, Qingdao, Shandong Province 266042, China.

¶(P.Y.) Department of Chemistry, Yale University, 225 Prospect Street, P.O. Box 208107, New Haven, CT 06520−8107, United States.

Notes

The authors declare no competing financial interest.

ACKNOWLEDGMENTS

M. Bacalum and M. Ameloot thank Dr. Ellen Gielen for support with the GUV preparations and Professor C. Richter-Landsberg (University of Oldenburg, Germany) for the OLN-93 cell line. M. Ameloot acknowledges the Province of Limburg (Belgium) for the financial support within the tUL IMPULS FASE II program allowing for the upgrading the laser source used in this work. S. Knippenberg is grateful to the European Marie Curie (COFUND) program along with the Belgian science policy office (BELSPO) for his funding as a postdoctoral research associate at the University of Mons between 2011 and 2013. P. Trouillas and G. Fabre thank the Conseil Régional du Limousin. D. Beljonne is a FNRS Research Director. P. Trouillas thanks the Czech Science Foundation (P208/12/G016). D. Beljonne and M. Ameloot thank BELSPO for the support received within the IAP-PAI P6/27 Functional Supramolecular Systems project. M. Ameloot acknowledges the Flemish Research Fund (FWO) supporting the Research Community of Microscopy. Mass spectrometry was made possible by the support of the Hercules Foundation of the Flemish Government (Grant 20100225-7).

REFERENCES

(1) Treibs, A.; Kreuzer, F.-H. Difluorboryl-Komplexe von Di- und Tripyrrylmethenen. *Justus Liebigs Ann. Chem.* **1968**, *718*, 208−223.

(2) Loudet, A.; Burgess, K. BODIPY dyes and their derivatives: Syntheses and spectroscopic properties. *Chem. Rev.* **2007**, *107* (11), 4891−4932.

(3) Ulrich, G.; Ziessel, R.; Harriman, A. The chemistry of fluorescent bodipy dyes: Versatility unsurpassed. *Angew. Chem., Int. Ed.* **2008**, *47* (7), 1184−1201.

(4) Boens, N.; Leen, V.; Dehaen, W. Fluorescent indicators based on BODIPY. *Chem. Soc. Rev.* **2012**, *41* (3), 1130−72.

(5) Boens, N.; Verbelen, B.; Dehaen, W. Postfunctionalization of the BODIPY core. Synthesis and spectroscopy. *Eur. J. Org. Chem.* **2015**, *2015*, 6577.

(6) Maier, O.; Oberle, V.; Hoekstra, D. Fluorescent lipid probes: some properties and applications (a review). *Chem. Phys. Lipids* **2002**, *116* (1−2), 3−18.

(7) Zhai, X. H.; Boldyrev, I. A.; Mizuno, N. K.; Momsen, M. M.; Molotkovsky, J. G.; Brockman, H. L.; Brown, R. E. Nanoscale Packing Differences in Sphingomyelin and Phosphatidylcholine Revealed by BODIPY Fluorescence in Mono layers: Physiological Implications. *Langmuir* **2014**, *30* (11), 3154−3164.

(8) Olšinová, M.; Jurkiewicz, P.; Pozník, M.; Šachl, R.; Prausová, T.; Hof, M.; Kozmík, V.; Teplý, F.; Svoboda, J.; Cebecauer, M. Di- and trioxalkyl derivatives of a boron dipyrromethene (BODIPY) rotor dye in lipid bilayers. *Phys. Chem. Chem. Phys.* **2014**, *16* (22), 10688−10697.

(9) Šachl, R.; Mikhalyov, I.; Gretskaya, N.; Olżyńska, A.; Hof, M.; Johansson, L. B. A. Distribution of BODIPY-labelled phosphatidyle-

DOI: 10.1021/acs.langmuir.6b00478
Langmuir 2016, 32, 3495−3505

thanolamines in lipid bilayers exhibiting different curvatures. *Phys. Chem. Chem. Phys.* **2011**, *13* (24), 11694−11701.
(10) Kaiser, R. D.; London, E. Determination of the depth of BODIPY probes in model membranes by parallax analysis of fluorescence quenching. *Biochim. Biophys. Acta, Biomembr.* **1998**, *1375* (1−2), 13−22.
(11) Dahim, M.; Mizuno, N. K.; Li, X. M.; Momsen, W. E.; Momsen, M. M.; Brockman, H. L. Physical and photophysical characterization of a BODIPY phosphatidylcholine as a membrane probe. *Biophys. J.* **2002**, *83* (3), 1511−1524.
(12) Li, Z.; Mintzer, E.; Bittman, R. First synthesis of free cholesterol-BODIPY conjugates. *J. Org. Chem.* **2006**, *71* (4), 1718−21.
(13) Boldyrev, I. A.; Zhai, X.; Momsen, M. M.; Brockman, H. L.; Brown, R. E.; Molotkovsky, J. G. New BODIPY lipid probes for fluorescence studies of membranes. *J. Lipid Res.* **2007**, *48* (7), 1518−32.
(14) Marks, D. L.; Bittman, R.; Pagano, R. E. Use of Bodipy-labeled sphingolipid and cholesterol analogs to examine membrane microdomains in cells. *Histochem. Cell Biol.* **2008**, *130* (5), 819−832.
(15) van Meer, G.; Voelker, D. R.; Feigenson, G. W. Membrane lipids: where they are and how they behave. *Nat. Rev. Mol. Cell Biol.* **2008**, *9* (2), 112−124.
(16) McMullen, T. P. W.; Lewis, R. N. A. H.; McElhaney, R. N. Cholesterol-phospholipid interactions, the liquid-ordered phase and lipid rafts in model and biological membranes. *Curr. Opin. Colloid Interface Sci.* **2004**, *8* (6), 459−468.
(17) Lakowicz, J. R. *Principles of Fluorescence Spectroscopy*, 3rd ed.; Springer-Verlag: New York, 2006.
(18) Knippenberg, S.; Bohnwagner, M. V.; Harbach, P. H.; Dreuw, A. Strong electronic coupling dominates the absorption and fluorescence spectra of covalently bound BisBODIPYs. *J. Phys. Chem. A* **2015**, *119* (8), 1323−31.
(19) Bacia, K.; Scherfeld, D.; Kahya, N.; Schwille, P. Fluorescence correlation spectroscopy relates rafts in model and native membranes. *Biophys. J.* **2004**, *87* (2), 1034−1043.
(20) Axelrod, D. Carbocyanine Dye Orientation in Red-Cell Membrane Studied by Microscopic Fluorescence Polarization. *Biophys. J.* **1979**, *26* (3), 557−573.
(21) Baumgart, T.; Hunt, G.; Farkas, E. R.; Webb, W. W.; Feigenson, G. W. Fluorescence probe partitioning between L-o/L-d phases in lipid membranes. *Biochim. Biophys. Acta, Biomembr.* **2007**, *1768* (9), 2182−2194.
(22) Kahya, N.; Scherfeld, D.; Bacia, K.; Poolman, B.; Schwille, P. Probing lipid mobility of raft-exhibiting model membranes by fluorescence correlation spectroscopy. *J. Biol. Chem.* **2003**, *278* (30), 28109−28115.
(23) Scherfeld, D.; Kahya, N.; Schwille, P. Lipid dynamics and domain formation in model membranes composed of ternary mixtures of unsaturated and saturated phosphatidylcholines and cholesterol. *Biophys. J.* **2003**, *85* (6), 3758−3768.
(24) Goud, T. V.; Tutar, A.; Biellmann, J. F. Synthesis of 8-heteroatom-substituted 4,4-difluoro-4-bora-3*a*, 4*a*-diaza-*s*-indacene dyes (BODIPY). *Tetrahedron* **2006**, *62* (21), 5084−5091.
(25) Boens, N.; Wang, L.; Leen, V.; Yuan, P.; Verbelen, B.; Dehaen, W.; Van der Auweraer, M.; De Borggraeve, W. D.; Van Meervelt, L.; Jacobs, J.; Beljonne, D.; Tonnelé, C.; Lazzaroni, R.; Ruedas-Rama, M. J.; Orte, A.; Crovetto, L.; Talavera, E. M.; Alvarez-Pez, J. M. 8-HaloBODIPYs and Their 8-(C, N, O, S) Substituted Analogues: Solvent Dependent UV-Vis Spectroscopy, Variable Temperature NMR, Crystal Structure Determination, and Quantum Chemical Calculations. *J. Phys. Chem. A* **2014**, *118* (9), 1576−94.
(26) Roacho, R. I.; Metta-Magaña, A.; Portillo, M. M.; Peña-Cabrera, E.; Pannell, K. H. 8-Amino-BODIPYs: Structural Variation, Solvent-Dependent Emission, and VT NMR Spectroscopic Properties of 8-R2N-BODIPY. *J. Org. Chem.* **2013**, *78* (9), 4245−4250.
(27) Osorio-Martínez, C. A.; Urías-Benavides, A.; Gómez-Durán, C. F. A.; Bañuelos, J.; Esnal, I.; López Arbeloa, I.; Peña-Cabrera, E. 8-AminoBODIPYs: Cyanines or Hemicyanines? The Effect of the Coplanarity of the Amino Group on Their Optical Properties. *J. Org. Chem.* **2012**, *77* (12), 5434−5438.
(28) Bañuelos, J.; Martín, V.; Gómez-Durán, C. F. A.; Arroyo Córdoba, I. J.; Peña-Cabrera, E.; García-Moreno, I.; Costela, Á.; Pérez-Ojeda, M. E.; Arbeloa, T.; López Arbeloa, I. New 8-Amino-BODIPY Derivatives: Surpassing Laser Dyes at Blue-Edge Wavelengths. *Chem.−Eur. J.* **2011**, *17* (26), 7261−7270.
(29) Leen, V.; Yuan, P. J.; Wang, L. N.; Boens, N.; Dehaen, W. Synthesis of Meso-Halogenated BODIPYs and Access to Meso-Substituted Analogues. *Org. Lett.* **2012**, *14* (24), 6150−6153.
(30) Braslavsky, S. E. Glossary of terms used in Photochemistry. *Pure Appl. Chem.* **2007**, *79* (3), 293−465.
(31) Gómez-Durán, C. F. A.; García-Moreno, I.; Costela, Á.; Martín, V.; Sastre, R.; Bañuelos, J.; López Arbeloa, F.; López Arbeloa, I.; Peña-Cabrera, E. 8-PropargylaminoBODIPY: unprecedented blue-emitting pyrromethene dye. Synthesis, photophysics and laser properties. *Chem. Commun.* **2010**, *46* (28), 5103−5105.
(32) Catalán, J. Toward a Generalized Treatment of the Solvent Effect Based on Four Empirical Scales: Dipolarity (SdP, a New Scale), Polarizability (SP), Acidity (SA), and Basicity (SB) of the Medium. *J. Phys. Chem. B* **2009**, *113* (17), 5951−5960.
(33) Koynova, R.; Caffrey, M. Phases and phase transitions of the phosphatidylcholines. *Biochim. Biophys. Acta, Rev. Biomembr.* **1998**, *1376* (1), 91−145.
(34) Li, L.; Cheng, J. X. Coexisting stripe- and patch-shaped domains in giant unilamellar vesicles. *Biochemistry* **2006**, *45* (39), 11819−11826.
(35) Wesołowska, O.; Michalak, K.; Maniewska, J.; Hendrich, A. B. Giant unilamellar vesicles - a perfect tool to visualize phase separation and lipid rafts in model systems. *Acta Biochim. Polym.* **2009**, *56* (1), 33−9.
(36) Juhasz, J.; Davis, J. H.; Sharom, F. J. Fluorescent probe partitioning in giant unilamellar vesicles of 'lipid raft' mixtures. *Biochem. J.* **2010**, *430* (3), 415−23.
(37) Ariola, F. S.; Mudaliar, D. J.; Walvick, R. P.; Heikal, A. A. Dynamics imaging of lipid phases and lipid-marker interactions in model biomembranes. *Phys. Chem. Chem. Phys.* **2006**, *8* (39), 4517−4529.
(38) Niemelä, P. S.; Ollila, S.; Hyvönen, M. T.; Karttunen, M.; Vattulainen, I. Assessing the nature of lipid raft membranes. *PLoS Comput. Biol.* **2007**, *3* (2), 304−312.
(39) Gullapalli, R. R.; Demirel, M. C.; Butler, P. J. Molecular dynamics simulations of DiI-C18(3) in a DPPC lipid bilayer. *Phys. Chem. Chem. Phys.* **2008**, *10* (24), 3548−60.
(40) Song, K. C.; Livanec, P. W.; Klauda, J. B.; Kuczera, K.; Dunn, R. C.; Im, W. Orientation of Fluorescent Lipid Analogue BODIPY-PC to Probe Lipid Membrane Properties: Insights from Molecular Dynamics Simulations. *J. Phys. Chem. B* **2011**, *115* (19), 6157−6165.
(41) Košinová, P.; Berka, K.; Wykes, M.; Otyepka, M.; Trouillas, P. Positioning of Antioxidant Quercetin and Its Metabolites in Lipid Bilayer Membranes: Implication for Their Lipid-Peroxidation Inhibition. *J. Phys. Chem. B* **2012**, *116* (4), 1309−1318.
(42) Paloncýová, M.; Berka, K.; Otyepka, M. Convergence of Free Energy Profile of Coumarin in Lipid Bilayer. *J. Chem. Theory Comput.* **2012**, *8* (4), 1200−1211.
(43) Marrink, S. J.; Berendsen, H. J. C. Simulation of Water Transport through a Lipid-Membrane. *J. Phys. Chem.* **1994**, *98* (15), 4155−4168.
(44) Humpoličková, J.; Gielen, E.; Benda, A.; Fagulova, V.; Vercammen, J.; Vandeven, M.; Hof, M.; Ameloot, M.; Engelborghs, Y. Probing diffusion laws within cellular membranes by Z-scan fluorescence correlation spectroscopy. *Biophys. J.* **2006**, *91* (3), L23−L25.
(45) Packard, B. S.; Wolf, D. E. Fluorescence Lifetimes of Carbocyanine Lipid Analogs in Phospholipid-Bilayers. *Biochemistry* **1985**, *24* (19), 5176−5181.
(46) Cabrini, G.; Verkman, A. S. Mechanism of interaction of the cyanine dye diS-C3-(5) with renal brush-border vesicles. *J. Membr. Biol.* **1986**, *90* (2), 163−75.

DOI: 10.1021/acs.langmuir.6b00478
Langmuir 2016, 32, 3495−3505

(47) Das, T. K.; Periasamy, N.; Krishnamoorthy, G. Mechanism of response of potential-sensitive dyes studied by time-resolved fluorescence. *Biophys. J.* **1993**, *64* (4), 1122−32.
(48) Kinosita, K., Jr.; Kawato, S.; Ikegami, A. A theory of fluorescence polarization decay in membranes. *Biophys. J.* **1977**, *20* (3), 289−305.
(49) Ameloot, M.; Hendrickx, H.; Herreman, W.; Pottel, H.; Vancauwelaert, F.; Vandermeer, W. Effect of Orientational Order on the Decay of the Fluorescence Anisotropy in Membrane Suspensions - Experimental-Verification on Unilamellar Vesicles and Lipid Alpha-Lactalbumin Complexes. *Biophys. J.* **1984**, *46* (4), 525−539.
(50) Timr, Š.; Brabec, J.; Bondar, A.; Ryba, T.; Železný, M.; Lazar, J.; Jungwirth, P. Nonlinear Optical Properties of Fluorescent Dyes Allow for Accurate Determination of Their Molecular Orientations in Phospholipid Membranes. *J. Phys. Chem. B* **2015**, *119* (30), 9706−9716.
(51) Gielen, E.; Smisdom, N.; vandeVen, M.; De Clercq, B.; Gratton, E.; Digman, M.; Rigo, J. M.; Hofkens, J.; Engelborghs, Y.; Ameloot, M. Measuring Diffusion of Lipid-like Probes in Artificial and Natural Membranes by Raster Image Correlation Spectroscopy (RICS): Use of a Commercial Laser-Scanning Microscope with Analog Detection. *Langmuir* **2009**, *25* (9), 5209−5218.
(52) Chiantia, S.; Ries, J.; Schwille, P. Fluorescence correlation spectroscopy in membrane structure elucidation. *Biochim. Biophys. Acta, Biomembr.* **2009**, *1788* (1), 225−233.
(53) Loura, L. M.; Fedorov, A.; Prieto, M. Partition of membrane probes in a gel/fluid two-component lipid system: a fluorescence resonance energy transfer study. *Biochim. Biophys. Acta, Biomembr.* **2000**, *1467* (1), 101−12.
(54) Sengupta, P.; Holowka, D.; Baird, B. Fluorescence resonance energy transfer between lipid probes detects nanoscopic heterogeneity in the plasma membrane of live cells. *Biophys. J.* **2007**, *92* (10), 3564−74.
(55) Chen, H.; Kim, S.; Li, L.; Wang, S.; Park, K.; Cheng, J. X. Release of hydrophobic molecules from polymer micelles into cell membranes revealed by Forster resonance energy transfer imaging. *Proc. Natl. Acad. Sci. U. S. A.* **2008**, *105* (18), 6596−601.
(56) Chen, H.; Kim, S.; He, W.; Wang, H.; Low, P. S.; Park, K.; Cheng, J. X. Fast release of lipophilic agents from circulating PEG-PDLLA micelles revealed by in vivo forster resonance energy transfer imaging. *Langmuir* **2008**, *24* (10), 5213−7.

DOI: 10.1021/acs.langmuir.6b00478
Langmuir 2016, 32, 3495−3505